DNA Nanotechnology Hot Paper

Deutsche Ausgabe: DOI: 10.1002/ange.201507375
Internationale Ausgabe: DOI: 10.1002/anie.201507375

A Case Study of the Likes and Dislikes of DNA and RNA in Self-Assembly

Hua Zuo, Siyu Wu, Mo Li, Yulin Li, Wen Jiang, and Chengde Mao**

Abstract: *Programmed self-assembly of nucleic acids (DNA and RNA) is an active research area as it promises a general approach for nanoconstruction. Whereas DNA self-assembly has been extensively studied, RNA self-assembly lags much behind. One strategy to boost RNA self-assembly is to adapt the methods of DNA self-assembly for RNA self-assembly because of the chemical and structural similarities of DNA and RNA. However, these two types of molecules are still significantly different. To enable the rational design of RNA self-assembly, a thorough examination of their likes and dislikes in programmed self-assembly is needed. The current work begins to address this task. It was found that similar, two-stranded motifs of RNA and DNA lead to similar, but clearly different nanostructures.*

Programmed DNA self-assembly has been extensively studied over the past three decades and successfully applied in the construction of a wide range of nanostructures.[1–25] The resulting structures have helped to address different problems, including molecular computation, nanofabrication, organizing nano-objects, drug delivery, structural studies of proteins, synthesis of artificial membrane channels, and probing biological processes. In contrast, programmed RNA self-assembly is less developed,[26–28] but holds greater promise as RNA has a wide array of structural motifs and functionalities. Incorporating such elements would potentially allow the construction of complicated and functional nanomachines. Given that RNA and DNA have similar chemical structures and both adopt a double-helix conformation, one question naturally arises: Can the methods developed for programmed DNA self-assembly be applied for the assembly of RNA nanostructures? The answer is clearly yes.[29–31] Mimicking DNA motifs, RNA nanomotifs have been constructed and successfully assembled into even larger nanostructures. However, do the corresponding DNA and RNA motifs always behave in the same fashion? To answer this critical question and to gain a complete set of engineering rules for programmed RNA self-assembly, it is necessary to systematically study the differences of RNA and DNA in terms of self-assembly as we did in this work.

Recently, we developed a simple, two-stranded RNA motif that can self-assemble into a homo-octameric RNA nanoprism (Figure 1e).[32] Herein, we examined the assembly behavior of the same two-stranded motif, but in this case, it is composed of DNA. An array of techniques, including native polyacrylamide gel electrophoresis (PAGE), atomic force microscopy (AFM), and cryogenic electron microscopy (cryo-EM), were applied for structural characterization. The experimental data turned out to be a surprise: Such a DNA motif self-assembles into a homo-hexameric, instead of a homo-octameric, DNA nanoprism. The assembly of octameric DNA nanoprisms requires two unique versions of such DNA motifs. This work highlights that these motifs (DNA and RNA) behave similarly in self-assembly, but still significantly different from each other.

The molecular design and the assembly strategy are illustrated in Figure 1. The basic building motif (Mn; $n = 1$–3) is a DNA duplex with internal single-strand loops (Lg and Lc, shown in green and cyan) and single-strand tails (Tc and Tr, shown in cyan and red). The cyan tail Tc and the cyan loop Lc are complementary to each other; upon hybridization, they form a T-junction.[33–37] Three tiles can associate with each other to form a triangle by T-junction formation (Figure 1b,c). The single-strand green loop (Lg) provides enough flexibility to allow the DNA duplex to bend. The red tail Tr (Figure 1b–d) is self-complementary and can self-dimerize, leading to the formation of triangular prisms (P1 and P2). Formation of a tetragonal prism requires two different motifs, M3a and M3b. Their overall structures are the same as those of M1 and M2, but the sequences of the T-junction-forming tails and loops were modified so that the cyan tail Tc is complementary to the cyan loop Lc, and the purple tail Tp is complementary to the purple loop Lp. Therefore, neither motif M3a nor motif M3b can self-oligomerize by T-junction formation; instead, they can only form cross-motif T-junctions, leading to the formation of a tetrameric square in which the motifs M3a and M3b are alternatingly arranged. Further dimerization through the red tail Tr will result in a tetragonal prism. Each motif can interact with three other motifs by T-junction formation or sticky-end hybridization. All inter-tile cohesions have similar stabilities and thus happen simultaneously during the assembly process rather than sequentially. It should also be pointed out that each motif contains two different DNA strands.

The assembly was conducted in a one-pot process. DNA strands were dissolved in a Mg^{2+} containing, neutral, aqueous buffer. The nanoprisms spontaneously assembled upon slowly

[*] H. Zuo
College of Pharmaceutical Sciences, Southwest University
Chongqing, 400716 (P.R. China)
E-mail: zuohua@swu.edu.cn
H. Zuo, S. Wu, M. Li, Y. Li, C. Mao
Department of Chemistry, Purdue University
West Lafayette, IN 47907 (USA)
E-mail: mao@purdue.edu
W. Jiang
Department of Biological Sciences, Purdue University
West Lafayette, IN 47907 (USA)

Supporting information for this article is available on the WWW under http://dx.doi.org/10.1002/anie.201507375.

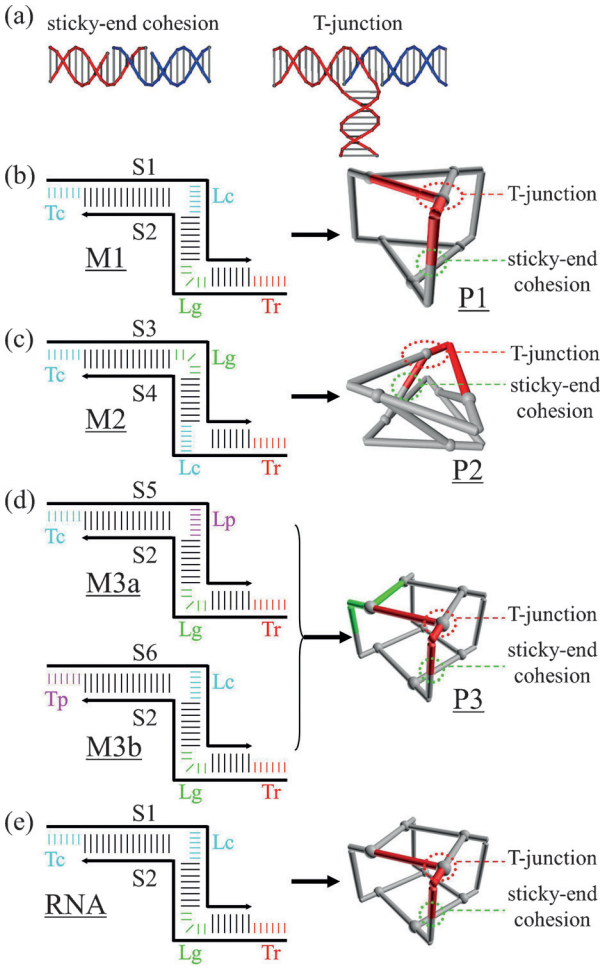

Figure 1. Different assembly behaviors of two-stranded DNA and RNA motifs. a) Two different cohesion methods. Each can be used for the association of two nucleic acid duplexes (red and blue). b–d) Three DNA nanoprisms (P*n*; $n=1$–3) and their corresponding building-block motifs (M*n*; $n=1$–3). In the prisms, one motif is highlighted in red or green. The homo-hexameric trigonal prisms P1 and P2 are assembled from the single motifs M1 and M2, respectively; the hetero-octameric tetragonal prism P3 is assembled from two different motifs, M3a and M3b. Each motif is a DNA duplex containing two internal loops, cyan loop Lc and green loop Lg, and two tails, cyan tail Tc and red tail Tr. The cyan Tc tail and the cyan Lc loop are complementary to each other and can associate into a T-junction. Red Tr is self-complementary, which allows for self-dimerization. The single-stranded Lg loop provides flexibility for the DNA duplex to bend. The thick lines indicate the backbone of the DNA strands and the short, thin lines indicate the bases or base pairs. e) The same motif made of RNA self-assembles into a homo-octameric tetragonal RNA prism.[32]

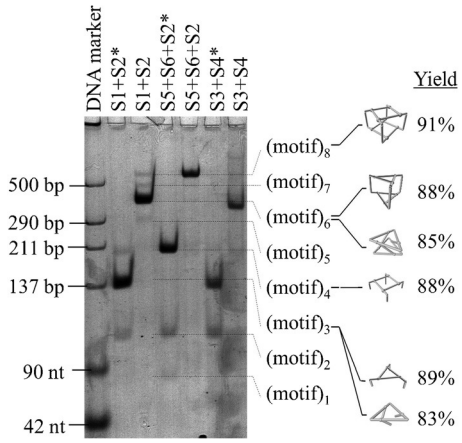

Figure 2. Analysis of DNA self-assembly by 5% PAGE. The DNA composition in each lane is indicated above the gel, and the chemical identity/structure geometry (and the corresponding assembly yield) of each band is given beside the gel. The strands S2* and S4* are identical to strands S2 and S4, respectively, except the absence of the self-complementary tail Tr.

cooling the DNA solutions from 95 °C to 4 °C over three hours. After assembly, the DNA samples were directly analyzed by PAGE (Figure 2; see also the Supporting Information, Figure S1). In each lane, a major band along with a series of very faint bands was visible. From those bands, the chemical compositions could be readily determined. A roughly linear relationship existed between the mobility and the logarithm of the molecular weight (Figure S4), which confirmed the assignment of the chemical composition. In each lane, the dominant, sharp band appeared to possess a mobility consistent with the expected DNA complex. To facilitate assigning the identity of each DNA complex, we also prepared DNA motifs lacking the self-complementary tail (Tr) from strand S*. Such DNA motifs can oligomerize through T-junctions to form triangles or squares, but cannot form prisms. Based on the band intensities, we used Image J, an image-processing software, to estimate the assembly yield of each major DNA complex. The yields were generally high (listed beside the corresponding structures).

We then visualized the DNA complexes with AFM, which further confirmed that all DNA nanostructures had been successfully assembled as designed. The three pseudo-planar structures were imaged in fluid to achieve high resolution (Figure 3). In Figure 3a and 3c, the expected triangle- and square-shaped geometries were observed, respectively, which verified our design and our assignment of the bands in Figure 2. In Figure 3b, the apparent particle shape was less clear. The branches at the T-junctions were flexible and pointed outward, making the complex to appear round. Furthermore, we imaged all DNA nanostructures by AFM in air (Figure 4) because the small 3D structures could not stably attach to the mica surface in fluid. In the AFM images, all DNA complexes appeared as individual particles. The 3D prisms were taller than the 2D objects, which is consistent with our design. Their apparent heights were approximately 1.3 nm for the pseudo-planar structures (triangles and squares) and about 2.3 nm for the 3D prisms. Owing to dehydration and strong electrostatic interactions, the 3D wireframe prisms would collapse on the mica surface.

To reveal the native 3D structure of the DNA complexes, we used cryo-EM imaging and 3D single-particle reconstruction,[38] which are powerful methods for studying the native 3D structures of biomacromolecules. The DNA complexes reported in this work are small porous frameworks, and each strut is one DNA duplex. Such structures have a low contrast in cryo-EM and present a challenge to cryo-EM imaging. Among these structures, the tetragonal prism is the largest

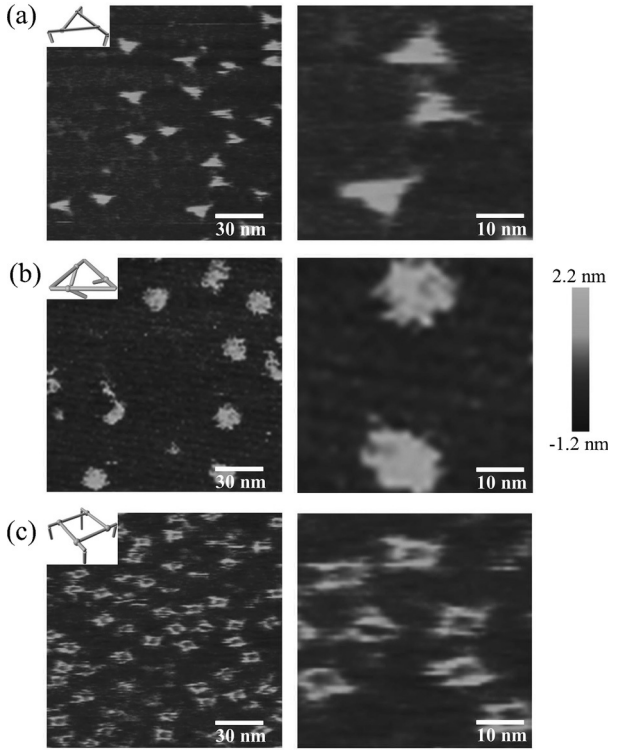

Figure 3. DNA pseudo-planar 2D nanostructures imaged by AFM in fluid. For each structure, a schematic representation is shown on the left. Two AFM images with different magnifications are shown for each structure. A height scale bar is shown on the right.

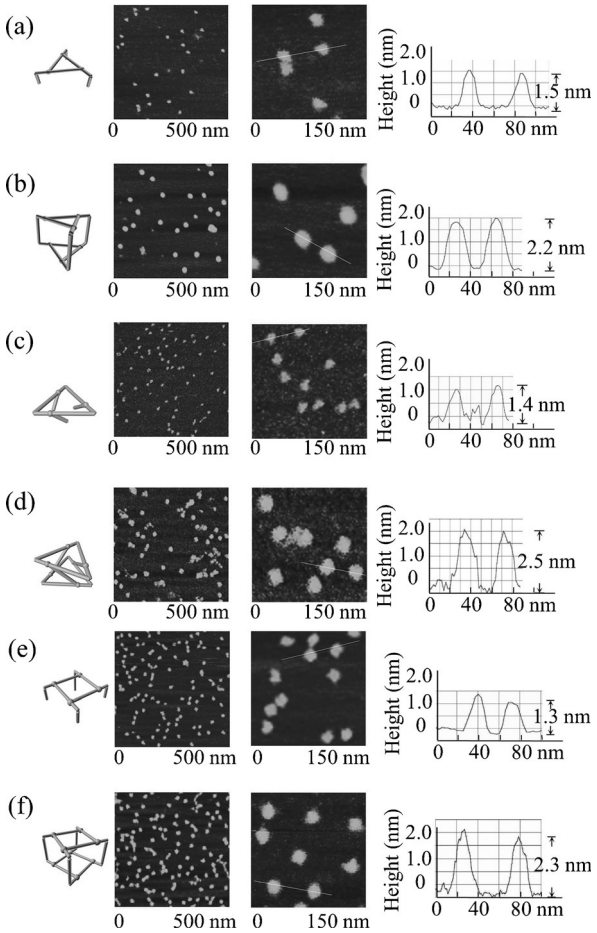

Figure 4. AFM images of the DNA nanostructures recorded in air. For each structure, a schematic representation is shown on the left, and two AFM images with different scales and a section analysis (along the line indicated in the AFM image with higher magnification) are shown on the right.

and partially overcomes the technical difficulties associated with cryo-EM imaging. It was thus chosen for detailed characterization studies (Figures 5, S2, and S3). In the raw images, individual particles with the expected sizes are randomly distributed. Based on these experimentally observed particles, the native 3D structure of the DNA complex was reconstructed at a resolution of 2.7 nm. It shows a twisted tetragonal prism, closely resembling the designed structure. From the reconstructed structural model, we back-calculated its 2D projections at different orientations and compared them with 1) the raw images of individual particles (Figure 5c) and 2) the class averages of raw images of particles at similar orientations (Figure S3). Clear similarities could be found in these comparisons, which confirmed that the assembled DNA complex indeed had a tetragonal-prism structure.

The current study and a previous study[32] make up a pair of studies that investigate the composition (DNA vs. RNA) effect for a simple two-stranded motif (Figure 1). Although they can both oligomerize by T-junction formation, they differ from each other significantly. The RNA motif forms a tetrameric square whereas the DNA motif forms a trimeric triangle. We speculate that this difference presumably originates from the helical geometric difference between the A-form (RNA) and B-form (DNA) duplexes (Figure S5 shows the structural models). In the A-form RNA duplex, the major groove is deep and can accommodate the branched duplex of the T-junction. Therefore, the T-junction is more structurally defined with a 90° angle, which leads to the formation of a square. In contrast, the B-form DNA duplex has a shallow major groove. The branched duplex of the T-junction is located outside the groove and is less structurally constrained; it thus has a higher degree of flexibility and can adapt the 60° angle necessary for triangle formation. Following this hypothesis, we reasoned that to assemble a DNA square, we could use two versions of the same motif (M3a and M3b) with different sequences (Figure 1d). In such a design, cyclization needs even numbers of motifs, and the motif is flexible enough to adopt the 90° angle needed for the formation of a square. This hypothesis has been confirmed by our experimental data.

In summary, we have investigated the composition effect (RNA vs. DNA) on the assembly behavior of a nucleic acid nanomotif. There are likes and dislikes between the two nucleic acids, DNA and RNA, in terms of programmed self-assembly. We cannot directly apply the strategies used for DNA nanotechnology to assemble RNA nanostructures, or vice versa. A thorough investigation of the composition effect is needed for further developing nucleic acid nanotechnology.

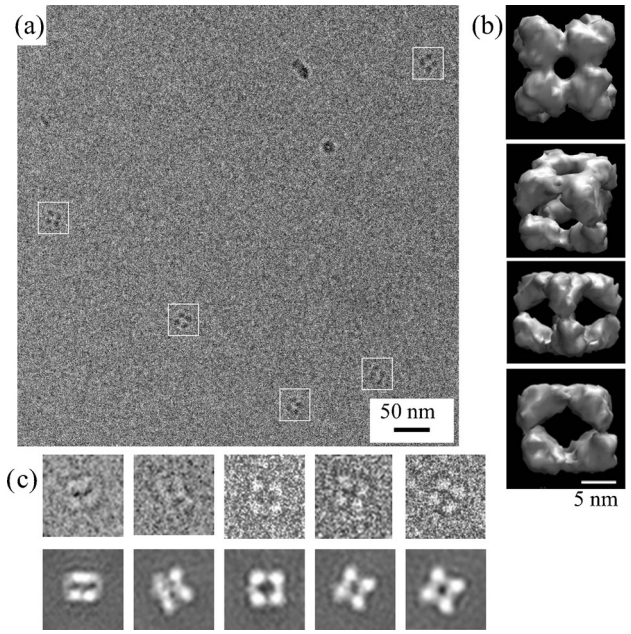

Figure 5. Cryo-EM of the self-assembled DNA tetragonal prism **P3**. a) A representative raw cryo-EM image of the DNA prism **P3**. White boxes indicate the DNA particles. b) Reconstructed structural model of the DNA complex viewed from different directions. c) Pairwise comparison between individual raw particles and the computer-generated 2D projections of the reconstructed 3D structural model in similar orientations.

Acknowledgements

We thank the NSF, the ONR (N00014-15-1-2707), and the NSFC (81429001) for support of this work. H.Z. was supported by the China Scholarship Council.

Keywords: atomic force microscopy · electron microscopy · DNA nanostructures · DNA nanotechnology · self-assembly

How to cite: *Angew. Chem. Int. Ed.* **2015**, *54*, 15118–15121
Angew. Chem. **2015**, *127*, 15333–15336

[1] E. Winfree, F. Liu, L. A. Wenzler, N. C. Seeman, *Nature* **1998**, *394*, 539–544.
[2] T. H. LaBean, H. Yan, J. Kopatsch, F. Liu, E. Winfree, J. H. Reif, N. C. Seeman, *J. Am. Chem. Soc.* **2000**, *122*, 1848–1860.
[3] H. Yan, S. H. Park, G. Finkelstein, J. H. Reif, T. H. LaBean, *Science* **2003**, *301*, 1882–1884.
[4] M. N. Hansen, A. M. Zhang, A. Rangnekar, K. M. Bompiani, J. D. Carter, K. V. Gothelf, T. H. LaBean, *J. Am. Chem. Soc.* **2010**, *132*, 14481–14486.
[5] J. Malo, J. C. Mitchell, A. J. Turberfield, *J. Am. Chem. Soc.* **2009**, *131*, 13574–13575.
[6] B. Wei, Y. Mi, *Biomacromolecules* **2005**, *6*, 2528–2532.
[7] B. Ding, R. Sha, N. C. Seeman, *J. Am. Chem. Soc.* **2004**, *126*, 10230–10231.
[8] Y. He, Y. Chen, H. Liu, A. E. Ribbe, C. Mao, *J. Am. Chem. Soc.* **2005**, *127*, 12202–12203.
[9] Y. He, Y. Tian, A. E. Ribbe, C. Mao, *J. Am. Chem. Soc.* **2006**, *128*, 15978–15979.
[10] Y. He, T. Ye, M. Su, C. Zhang, A. E. Ribbe, W. Jiang, C. Mao, *Nature* **2008**, *452*, 198–202.
[11] C. Tian, X. Li, Z. Liu, W. Jiang, G. Wang, C. Mao, *Angew. Chem. Int. Ed.* **2014**, *53*, 8041–8044; *Angew. Chem.* **2014**, *126*, 8179–8182.
[12] P. W. K. Rothemund, *Nature* **2006**, *440*, 297–302.
[13] E. S. Andersen, M. Dong, M. M. Nielsen, K. Jahn, R. Subramani, W. Mamdouh, M. M. Golas, B. Sander, H. Stark, C. L. P. Oliveira, J. S. Pedersen, V. Birkedal, F. Besenbacher, K. V. Gothelf, J. Kjems, *Nature* **2009**, *459*, 73–76.
[14] S. M. Douglas, H. Dietz, T. Liedl, B. Högberg, F. Graf, W. M. Shih, *Nature* **2009**, *459*, 414–418.
[15] H. Dietz, S. M. Douglas, W. M. Shih, *Science* **2009**, *325*, 725–730.
[16] D. Han, S. Pal, J. Nangreave, Z. Deng, Y. Liu, H. Yan, *Science* **2011**, *332*, 342–346.
[17] Y. Ke, S. M. Douglas, M. Liu, J. Sharma, A. Cheng, A. Leung, Y. Liu, W. M. Shih, H. Yan, *J. Am. Chem. Soc.* **2009**, *131*, 15903–15908.
[18] Y. Fu, D. Zeng, J. Chao, Y. Jin, Z. Zhang, H. Liu, D. Li, H. Ma, Q. Huang, K. V. Gothelf, C. Fan, *J. Am. Chem. Soc.* **2013**, *135*, 696–702.
[19] R. Schreiber, J. Do, E.-M. Roller, T. Zhang, V. J. Schüller, P. C. Nickels, J. Feldmann, T. Liedl, *Nat. Nanotechnol.* **2014**, *9*, 74–78.
[20] B. Wei, M. Dai, P. Yin, *Nature* **2012**, *485*, 623–626.
[21] Y. Ke, L. L. Ong, W. M. Shih, P. Yin, *Science* **2012**, *338*, 1177–1183.
[22] Y. Ke, L. L. Ong, W. Sun, J. Song, M. Dong, W. M. Shih, P. Yin, *Nat. Chem.* **2014**, *6*, 994–1002.
[23] N. C. Seeman, *Annu. Rev. Biochem.* **2010**, *79*, 65–87.
[24] F. Zhang, J. Nangreave, Y. Liu, H. Yan, *J. Am. Chem. Soc.* **2014**, *136*, 11198–11211.
[25] M. R. Jones, N. C. Seeman, C. A. Mirkin, *Science* **2015**, *347*, 1260901–12609011.
[26] P. Guo, *Nat. Nanotechnol.* **2010**, *5*, 833–842.
[27] W. W. Grabow, L. Jaeger, *Acc. Chem. Res.* **2014**, *47*, 1871–1880.
[28] K. A. Afonin, W. K. Kasprzak, E. Bindewald, M. Kireeva, M. Viard, M. Kashlev, B. A. Shapiro, *Acc. Chem. Res.* **2014**, *47*, 1731–1741.
[29] S. H. Ko, M. Su, C. Zhang, A. E. Ribbe, W. Jiang, C. Mao, *Nat. Chem.* **2010**, *2*, 1050–1055.
[30] P. Wang, S. H. Ko, C. Tian, C. Hao, C. Mao, *Chem. Commun.* **2013**, *49*, 5462–5464.
[31] M. Endo, S. Yamamoto, K. Tatsumi, T. Emura, K. Hidaka, H. Sugiyam, *Chem. Commun.* **2013**, *49*, 2879–2881.
[32] J. Yu, Z. Liu, W. Jiang, G. Wang, C. Mao, *Nat. Commun.* **2015**, *6*, 5724.
[33] S. Hamada, S. Murata, *Angew. Chem. Int. Ed.* **2009**, *48*, 6820–6823; *Angew. Chem.* **2009**, *121*, 6952–6955.
[34] C. Tian, C. Zhang, X. Li, C. Hao, S. Ye, C. Mao, *Langmuir* **2014**, *30*, 5859–5862.
[35] X. Li, C. Zhang, C. Hao, C. Tian, G. Wang, C. Mao, *ACS Nano* **2012**, *6*, 5138–5142.
[36] Z. Nie, P. Wang, C. Tian, C. Mao, *Angew. Chem. Int. Ed.* **2014**, *53*, 8402–8405; *Angew. Chem.* **2014**, *126*, 8542–8545.
[37] J. Lee, S. Hamada, R. Amin, S. Kim, A. Kulkarni, T. Kim, Y. Roh, S. Murata, S. H. Park, *Small* **2012**, *8*, 374–377.
[38] S. J. Ludtke, P. R. Baldwin, W. Chiu, *J. Struct. Biol.* **1999**, *128*, 82–97.

Received: August 7, 2015
Revised: September 10, 2015
Published online: October 12, 2015